Pergamon

0301-9322(95)00005-4

Int. J. Multiphase Flow Vol. 21, No. 4, pp. 621–637, 1995

0301-9322/95 $9.50 + 0.00

EXPERIMENTAL STUDY OF AIR–WATER TWO-PHASE FLOW THROUGH A FRACTURE (NARROW CHANNEL)

M. FOURAR and S. BORIES

Institut de Mécanique des Fluides de Toulouse, Avenue du Professeur Camille Soula, 31400 Toulouse, France

(Received 22 September 1994; in revised form 16 January 1995)

Abstract—Two-phase (air–water) flow experiments were conducted in artificial horizontal fractures (narrow channels). Two experimental set-ups were utilized. One set of experiments was performed by using two glass plates (1 × 0.5 m) with a gap width of 1 mm. The second set of experiments was performed using two bricks made of baked clay (28 × 14 cm) for which three gap widths of $h_1 = 0.54$ mm, $h_2 = 0.40$ mm and $h_3 = 0.18$ mm have been tested. Air and water were injected separately, through alternating capillary tubes for the first set-up and through a porous medium for the second. For each experiment, the fracture was initially saturated at constant water flow-rate, and air injection was then started. When steady state was reached, pressure drop and liquid volume fraction were measured. Then, air injection was increased stepwise and the experiment was repeated at different liquid flow rates. By varying the flow rates of each fluid phase, different flow structures were observed for the glass channel experiment: bubbles, fingering bubbles, complex, annular and droplet flow. These flow structures show more similarity to those observed in pipes than to those expected in porous media. Using the formalism developed for two-phase flow in pipes, and by taking experimental observations into account, a theoretical relationship for the two-phase pressure gradient is proposed. This relationship is evaluated with experimental data. Then, the results are analyzed with three models. First, the Lockhart & Matinelli model gives a good fit for both pressure drop and liquid volume fraction against the Martinelli parameter. Second, by considering the two phases flowing in the fracture as a single phase with averaged properties, the appropriate friction factor and Reynolds number of the mixture are defined. This model, which is similar to the homogeneous model, permits the selection of the experimental data corresponding to laminar flow. Finally, by using the generalized Darcy model, it was found that for laminar flow, the liquid-phase relative permeability is equal to the liquid volume fraction, while the gas-phase relative permeability is not a linear function of the liquid volume fraction.

Key Words: two-phase flow, fracture, channel, pressure drop, volume fraction

INTRODUCTION

Two-phase flow in fractures (narrow channels) is of great importance in several industrial processes (compact heat exchangers, nuclear engineering) and in several geophysical situations (oil reservoirs, geothermal energy). From a petroleum recovery and exploitation of geothermal energy viewpoint, the approach commonly used to describe steady state laminar two-phase flows in fractures is the generalized Darcy's law:

$$\mathbf{V}_L = -\frac{kKr_L}{\mu L}(\nabla P_L - \rho_L \boldsymbol{g}) \quad [1]$$

$$\mathbf{V}_G = -\frac{kKr_G}{\mu G}(\nabla P_G - \rho_G \boldsymbol{g}) \quad [2]$$

where subscripts L and G stand, respectively, for liquid and gas, V is the superficial velocity (or Darcy's velocity), ∇P the pressure gradient, μ the dynamic viscosity, ρ the fluid density, k the equivalent intrinsic permeability (single-phase flow) of the fracture, Kr the relative permeability and $\boldsymbol{g}$ the acceleration due to gravity. This law has never been theoretically justified. It is only based on the analogy between a single-phase flow in porous media and a single-phase flow in a Hele–Shaw cell, for which the equivalent intrinsic permeability is $k = h^2/12$, h being the gap width of the fracture.

Few experimental studies have been undertaken in order to verify [1] and [2] and to establish the relationship between relative permeabilities and the volume fraction. Romm (1966) studied two-phase flow of water and kerosene confined in different stripes of a smooth fracture by controlling the wettability of surfaces. The relative permeability of each phase is then equal to its volume fraction: $Kr_L = S_L$ and $Kr_G = S_G$, i.e. that no phase interfaces with the flow of the other. Consequently, $Kr_L + Kr_G = 1$. However, the generalization of this result was confirmed neither by the experimental works of Persoff *et al.* (1991, 1994) and Fourar *et al.* (1991, 1993), nor by the numerical simulations by Pruess & Tsang (1990) and Pyrak-Nolte *et al.* (1992). On the other hand, Ali *et al.* (1991) analyzed the effects of gap width and orientation on air–water two-phase flow in a narrow passage between two flat plates. As in Fourar *et al.* (1993), for every orientation, except for horizontal flow between vertical plates, both the void fraction and friction pressure drop have been correlated by using the model of Lockhart & Martinelli.

In this paper we report additional results concerning two-phase (air–water) flow in artificial horizontal fractures. Experimental set-ups are described in the first part. Then, results concerning flow structures, pressure gradients and liquid volume fractions are presented. Using the formalism developed for two-phase flow in pipes, and by taking experimental observations into account, a theoretical relationship for the two-phase pressure gradient is proposed. This relationship is evaluated with experimental data. Then, results are analyzed with three models: (1) Lockhart & Martinelli model, (2) an equivalent homogeneous model and (3) the generalized Darcy model.

EXPERIMENTAL SET-UP

The schematic of the experimental set-up is shown in figure 1. Two experimental set-ups were utilized. In the first set of experiments, the fracture consisted of two glass plates 1 m long and 0.5 m wide separated by 1-mm-thick strips of stainless steel along the outer boundaries. The injector consisted of 500 stainless steel tubes of 1 mm outside diameter and 0.66 mm inside diameter. Air and water were injected through alternating capillary tubes to achieve uniform distribution of the inlet flow. For the second set of experiments, the fracture consisted of two bricks made of baked clay (28 × 14 cm) for which three gap widths of $h_1 = 0.54$ mm, $h_2 = 0.40$ mm and $h_3 = 0.18$ mm have been tested. The injector consisted of a metallic box filled with glass beads of 1 mm-diameter.

For all experiments, air was injected at constant pressure and its volumetric flow rate was measured by a rotameter and corrected to the standard pressure. Water was injected by a calibrated pump. At the outlet of the fracture, the gas escaped to the atmosphere and the water was collected in a decanter and recycled. The fracture was initially saturated with water which was injected at a constant rate before each experiment. Air injection was then started and increased stepwise. When steady state was reached for each flow rate, the pressure drop and liquid volume fraction (in the case of the fracture made of glass only) were measured. Then the fracture was re-saturated with water and the experiment was repeated several times at different liquid flow rates.

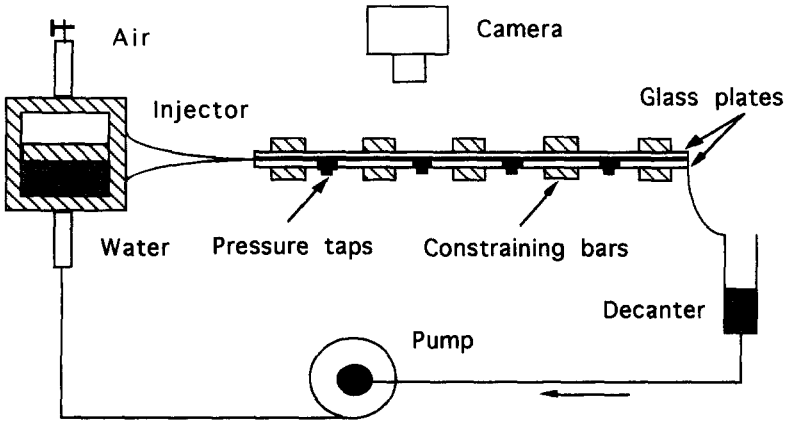

Figure 1. Experimental set-up.

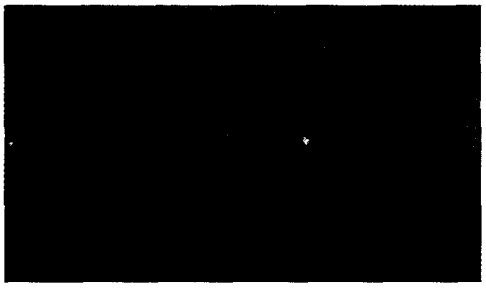

BUBBLE FLOW

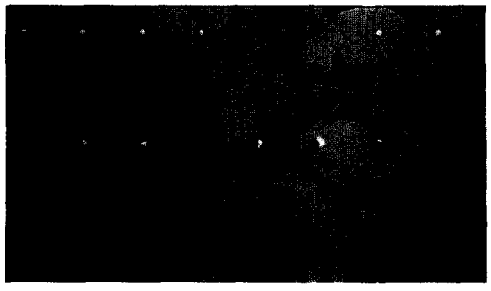

FINGERING BUBBLE FLOW

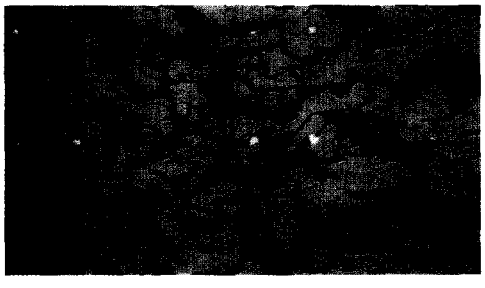

COMPLEX FLOW

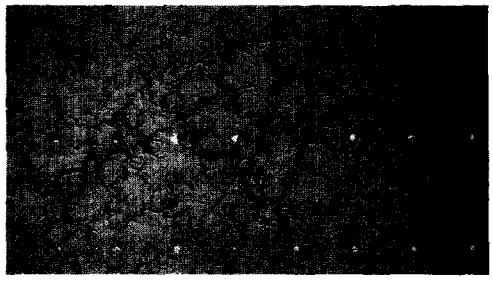

ANNULAR FLOW

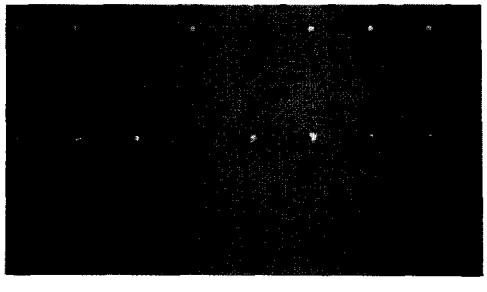

DROPLET FLOW

Figure 2. Photographs of flow structures observed in the glass channel. The flow is from left to right. The liquid contained dye and appears red while the gas appears light.

For the fracture made of glass, nine liquid-filled pressure taps were cemented into holes drilled along the center line of the lower plate. Any pair of taps could be connected by valves to a differential transducer. The pressure at any given tap fluctuated rapidly, due to the successive arrival of different fluid phases at the tap. Therefore, only the time-averaged values were recorded. The liquid volume fraction was measured by a volume balance method. The water volume in the decanter was measured at the beginning of the experiment with the fracture completely saturated with flowing water. Then it was re-measured at steady state for each given air flow rate. The variation of the water volume in the decanter was then used to calculate the liquid volume fraction in the fracture.

For the fracture made of baked clay, the pressure drop was measured by using two liquid-filled pressure taps cemented into holes at the inlet and the outlet of the fracture. Both taps were connected to a differential transducer. Because the volume of the fracture was very small, the liquid volume fraction was not measured.

The gap width of each fracture was calculated from laminar single-phase flow experiments obeying the cubic law:

$$\frac{dP}{dx} = -\frac{12\mu_L Q_L}{h^3} \qquad [3]$$

Q_L is the volumetric liquid flow rate per unit width and μ_L is the dynamic viscosity of the liquid-phase.

EXPERIMENTAL RESULTS

Flow structures

By varying the flow rate for each phase, different flow structures were observed for the glass channel: bubbles, fingering bubbles, complex, annular and droplet flow. These flow structures were constantly in motion, never stopping, even momentarily. Photographs of flow structures for the glass channel are presented in figure 2, and the flow map is presented in figure 3. For the clay channel, flow structures have not been visualized.

For a given liquid flow rate, at low gas flow rate we observed gas bubbles dispersed in the flowing liquid (bubbles flow). Increasing the gas flow rate increased the size of bubbles which started to

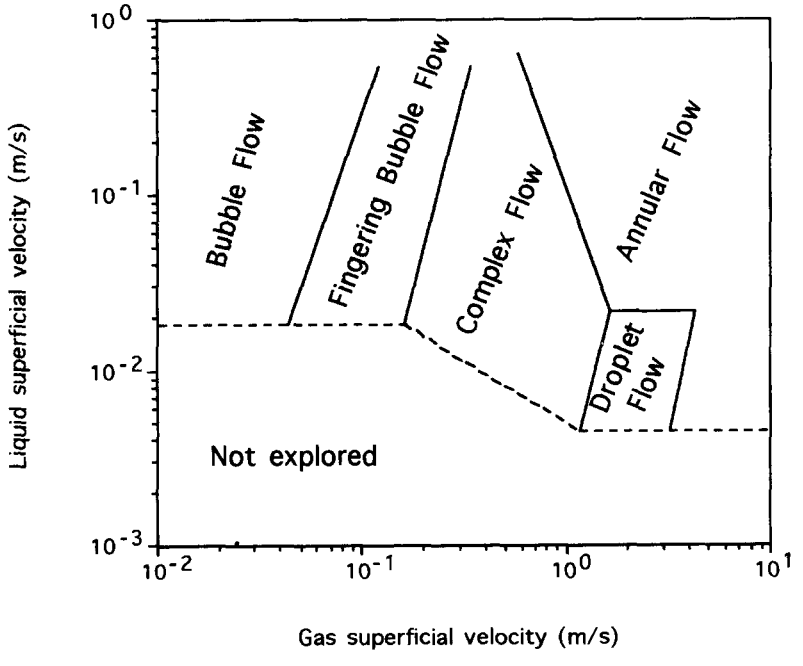

Figure 3. Flow map (glass channel).

become unstable by tip-splitting (fingering bubbles flow). Then when the gas flow rate was further increased, the flow became chaotic with no apparent structures (complex flow). At higher gas flow rates, the gas occupied the main part of the fracture, the liquid flowing as unstable films along the walls (annular flow). However, for low liquid velocities, films were replaced by liquid droplets dispersed in the flowing gas (dispersed droplet flow). Note that the flow structures described above, show more similarity to those observed in pipes than to those expected in porous media.

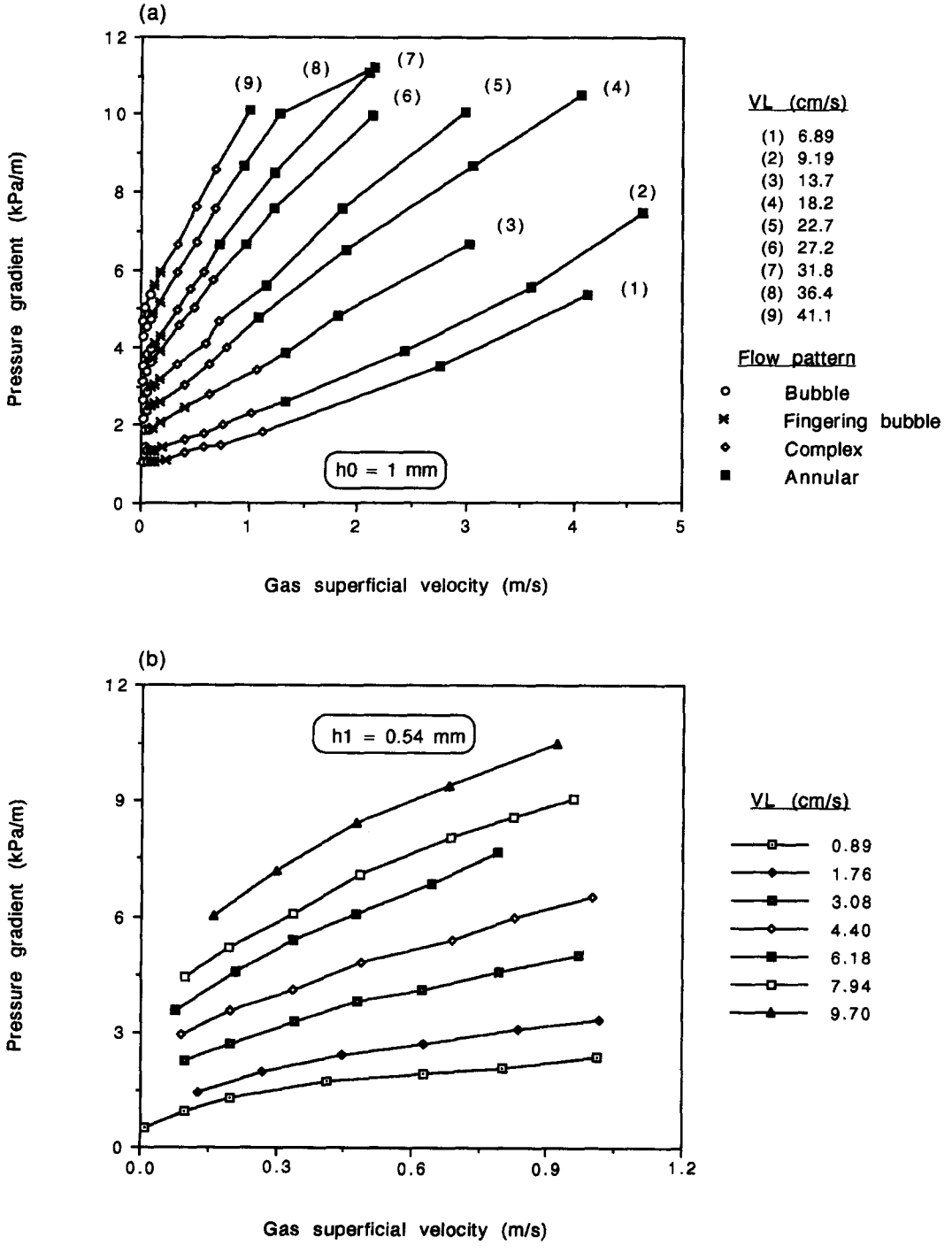

Fig. 4(a) and (b). *Caption overleaf.*

Two-phase pressure drops and liquid volume fractions

The measured two-phase pressure drops against gas superficial velocity are presented in figure 4(a), (b), (c) and (d) for all fractures. Different curves were obtained. Each curve represents an individual experiment in which the liquid flow rate was held constant and the gas flow rate was increased. The observed trend conforms to what is commonly observed for two-phase flow in pipes. Actually, for a given liquid superficial velocity, increasing the gas superficial velocity increased the

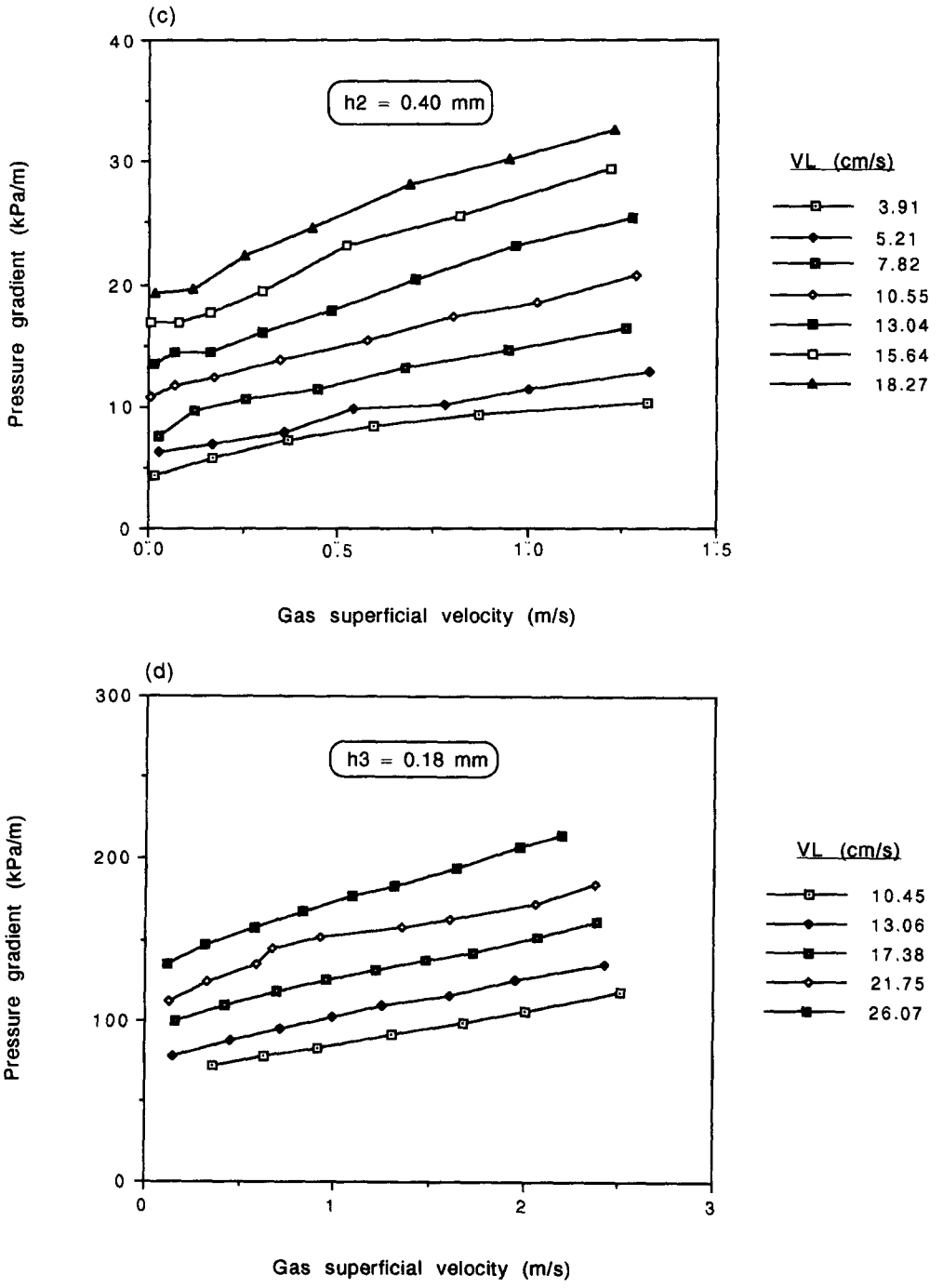

Fig. 4 (c) and (d)

Figure 4. Two-phase pressure gradient versus gas superficial velocity. (a) Fracture made of glass (h_0 = 1 mm); (b) fracture made of baked clay ($h_1 = 0.54$ mm); (c) fracture made of baked clay ($h_2 = 0.40$ mm); (d) fracture made of baked clay ($h_3 = 0.18$ mm).

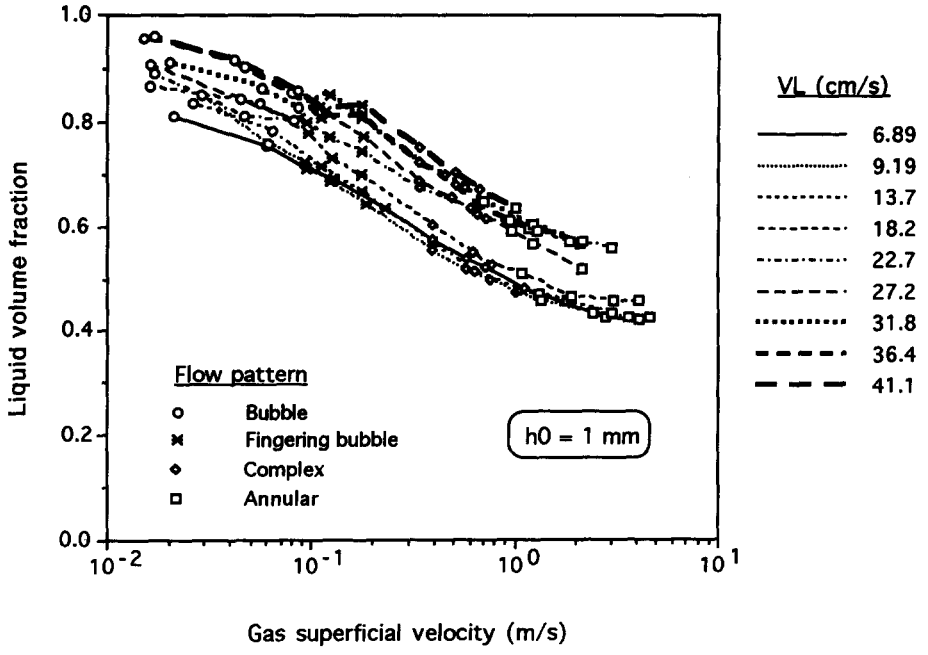

Figure 5. Liquid volume fraction against gas superficial velocity.

pressure drop. As shown in figure 4 (a), (b), (c) and (d), the pressure gradient is almost a linear function of the gas superficial velocity. Note that for the glass channel, there is no sharp variation in the pressure gradient when the flow structure changes, unlike flow in a pipe. Otherwise, for the clay channel and for given liquid and gas flow rates, the pressure drop increases when the gap width decreases as in single-phase flow, in accordance with the cubic law.

Measured liquid volume fractions for the glass channel versus gas superficial velocity are presented in figure 5. The observed trend conforms to what is commonly observed for two-phase flow in pipes. The overlapping of curves is due to errors of measurements of liquid volume fractions.

MACROSCOPIC LAWS

The modeling is based on the formalism developed for two-phase flow in pipes, Delhaye (1981):

$$S_L \frac{dP_L}{dx} - S_L \rho_L g_x = \frac{\pi_L}{A} \tau_L + \frac{\pi_0}{A} \tau_{L0} \quad [4]$$

$$S_G \frac{dP_G}{dx} - S_G \rho_G g_x = \frac{\pi_G}{A} \tau_G + \frac{\pi_0}{A} \tau_{G0} \quad [5]$$

where τ_{i0} ($i = L, G$) is the average interfacial shear stress, τ_i the average wall shear stress, π_0 the interfacial perimeter, π_i the wetted perimeter by phase i and A the channel area. In [4] and [5], π_L, π_G and π_0 indicate that the flow of each phase is not only dependent on the volume fraction but also on the flow structure. This is a fundamental distinction in comparison with the situation in classical porous media where, in consequence of the intervention of capillary forces, one supposes that no particular configuration exists to emphasize the interfacial phenomena. Equations [4] and [5] were solved taking into account the hypotheses suggested by the experiments:

(i) only the wet phase (water) is in contact with channel walls (figure 6), the wetted perimeter by each phase is then given by:

$$\pi_L = 2(w + h) \approx 2w \quad \text{and} \quad \pi_G = 0 \quad [6]$$

where w is the width of the channel ($A = w \times h$),

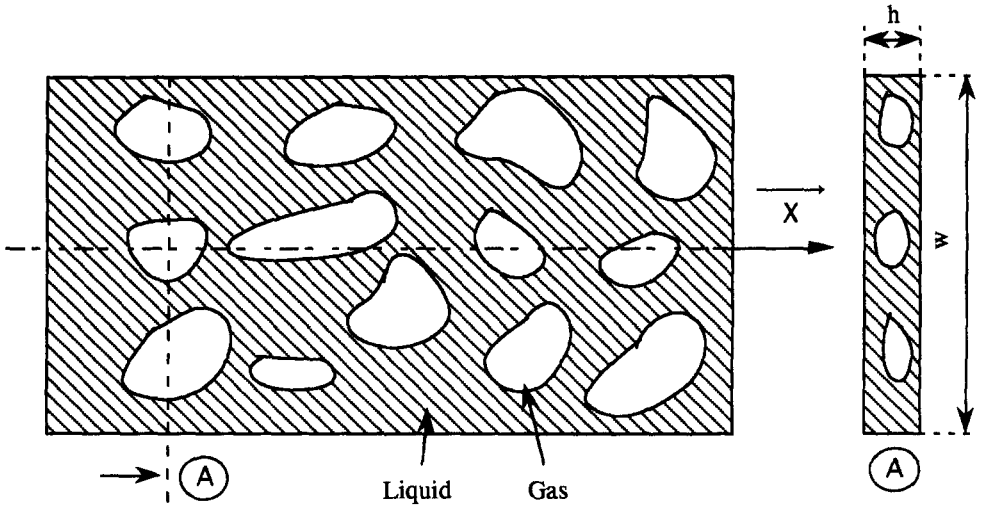

Figure 6. Schematic representation of two-phase configuration.

(ii) the capillary pressure is negligible, then the pressure gradient is uniform in each phase, and:

$$\tau_{L0} = -\tau_{G0} = \tau_0 \qquad [7]$$

Thus, the average wall shear stress is supposed to be given by:

$$\tau_L = -6\frac{\mu_L U_L}{h} \qquad [8]$$

where

$$U_L = \frac{V_L}{S_L} \qquad [9]$$

is the interstitial velocity, V_L being the superficial velocity. As shown in Coutris *et al.* (1989), the above hypotheses must be reconsidered for a two-layer flow.

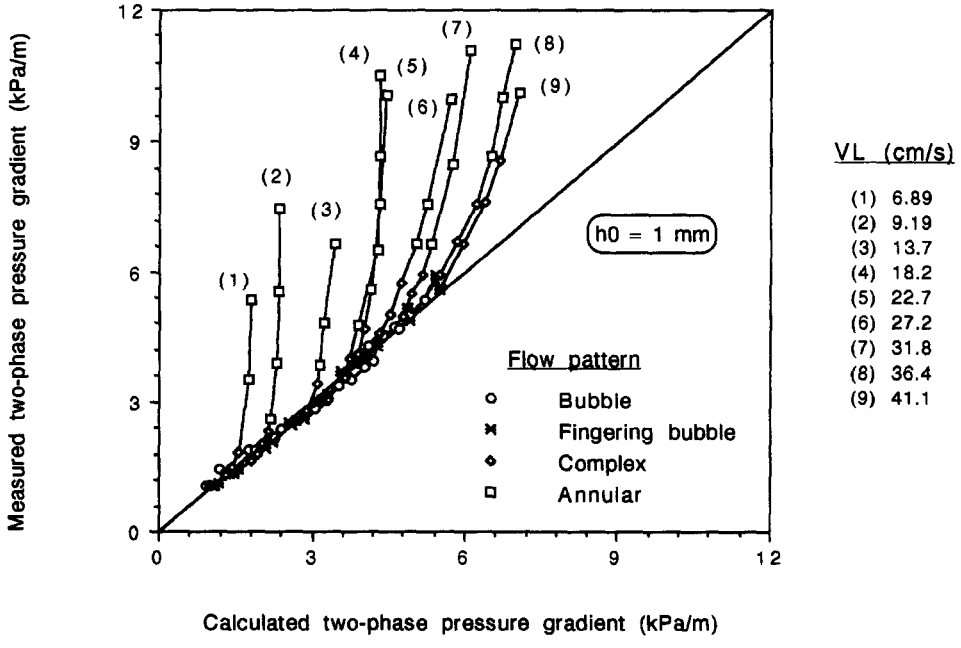

Figure 7. Comparison between measured and calculated pressure gradients by using [12] (glass channel).

Consequently, macroscopic laws governing the horizontal flow (no gravity) of the liquid-phase, gas-phase and two-phase mixture are, respectively, given by:

$$S_L \frac{dP}{dx} = -\frac{12\mu_L V_L}{h^2 S_L} + \frac{\pi_0}{A}\tau_0 \quad [10]$$

$$S_G \frac{dP}{dx} = -\frac{\pi_0}{A}\tau_0 \quad [11]$$

$$\frac{dP}{dx} = -\frac{12\mu_L V_L}{h^2 S_L} \quad [12]$$

For the glass channel, we have plotted in figure 7, the measured versus the calculated pressure gradient from [12]. Different curves were obtained. Each curve represents an individual experiment in which the liquid flow rate was held constant and the gas flow rate was increased. For a given liquid flow rate, at gas flow rates corresponding to bubbles, fingering bubbles and complex flow, the measured and calculated pressure gradients are equal. However, at higher gas flow rates (annular flow), the measured pressure gradient is higher than that predicted by [12]. This discrepancy is caused by inertial forces (see below).

LOCKHART & MARTINELLI MODEL

The model of Lockhart & Martinelli (1949), which was developed for two-phase flow in pipes, consists in dimensionless correlations between pressure gradient and flow rates of phases. Lockhart & Martinelli defined the following parameters:

—gas-phase friction multiplier:

$$\Phi_G = \sqrt{\frac{(dP/dx)}{(dP/dx)_G}} \quad [13]$$

—liquid-phase friction multiplier:

$$\Phi_L = \sqrt{\frac{(dP/dx)}{(dP/dx)_L}} \quad [14]$$

—Martinelli parameter:

$$X = \frac{\Phi_G}{\Phi_L} = \sqrt{\frac{(dP/dx)_L}{(dP/dx)_G}} \quad [15]$$

In these equations, (dP/dx) is the two-phase pressure gradient and $(dP/dx)_G$ and $(dP/dx)_L$ are, respectively, the gas and the liquid single-phase pressure gradients which would be obtained if each phase were flowing alone in the fracture with the same superficial velocity as under two-phase flow conditions. For a laminar–laminar flow regime, these pressure gradients are given by:

$$\left(\frac{dP}{dx}\right)_G = -\frac{12\mu_G V_G}{h^2} \quad [16]$$

$$\left(\frac{dP}{dx}\right)_L = -\frac{12\mu_L V_L}{h^2} \quad [17]$$

The Martinelli parameter is then given by:

$$X = \sqrt{\frac{\mu_L V_L}{\mu_G V_G}} \quad [18]$$

The plot of figure 8 displays Φ_G versus X for data obtained with the glass channel. This plot shows that, except for the annular flow configuration, there is a linear relationship between these parameters:

$$\Phi_G = 1 + X \quad [19]$$

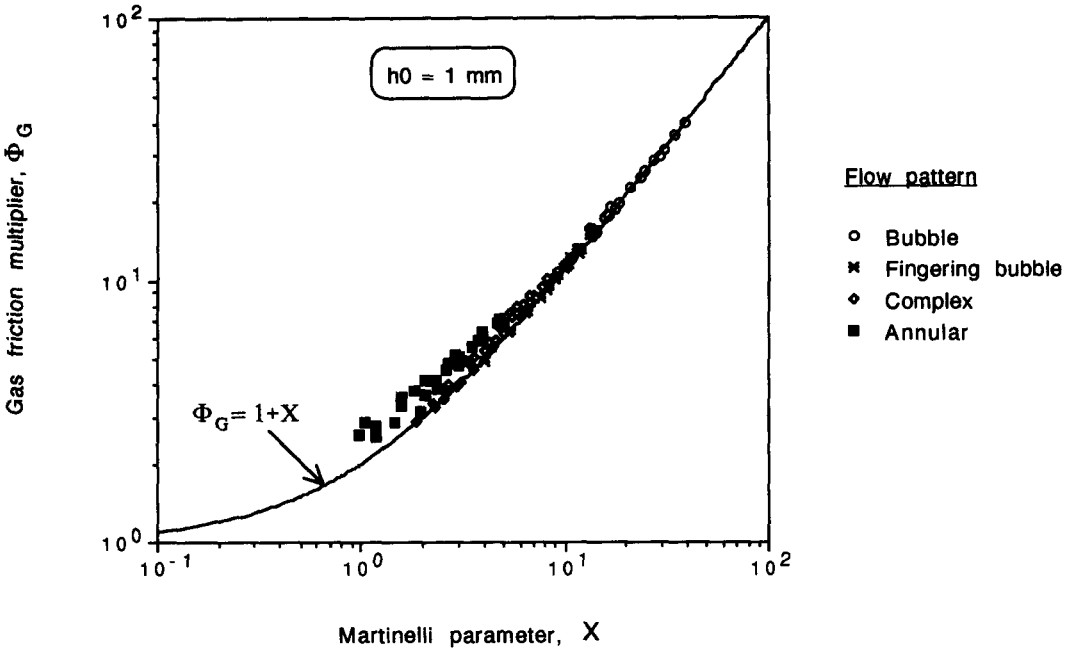

Figure 8. Gas friction multiplier vs Martinelli parameter (glass channel).

Equations [12] and [18] were obtained by assuming that the flow of each phase is laminar. The discrepancy observed between [19] and experimental data for the annular flow structure is caused by inertial forces. This will be verified in the next paragraph.

From [15] and [19], we deduce the expression for Φ_L:

$$\Phi_L = \frac{1+X}{X} \qquad [20]$$

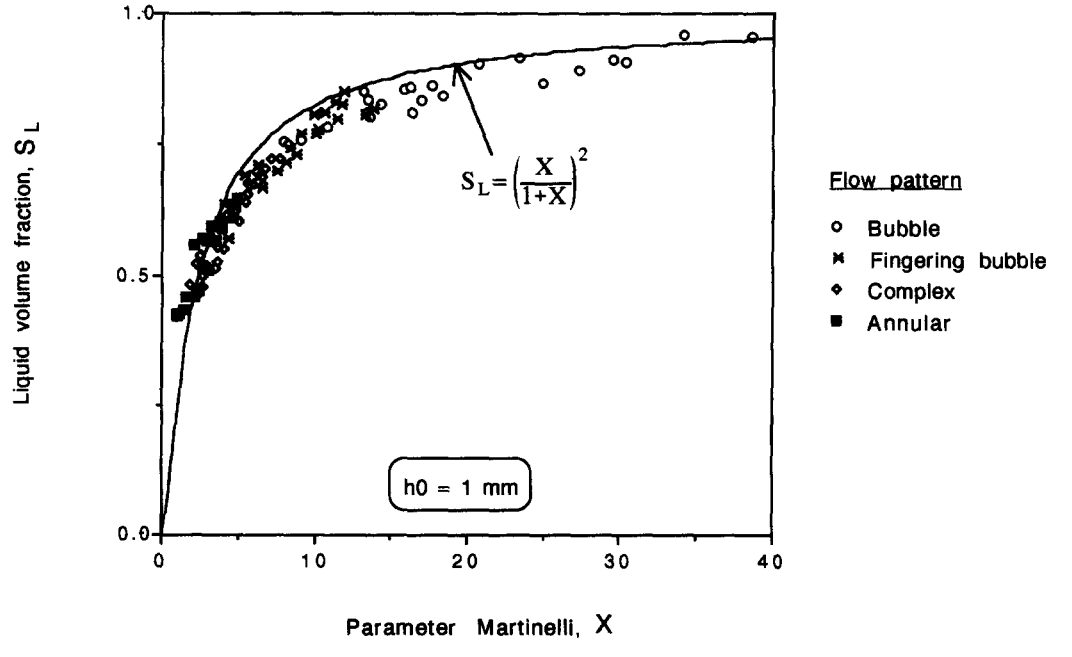

Figure 9. Liquid volume fraction vs Martinelli parameter (glass channel).

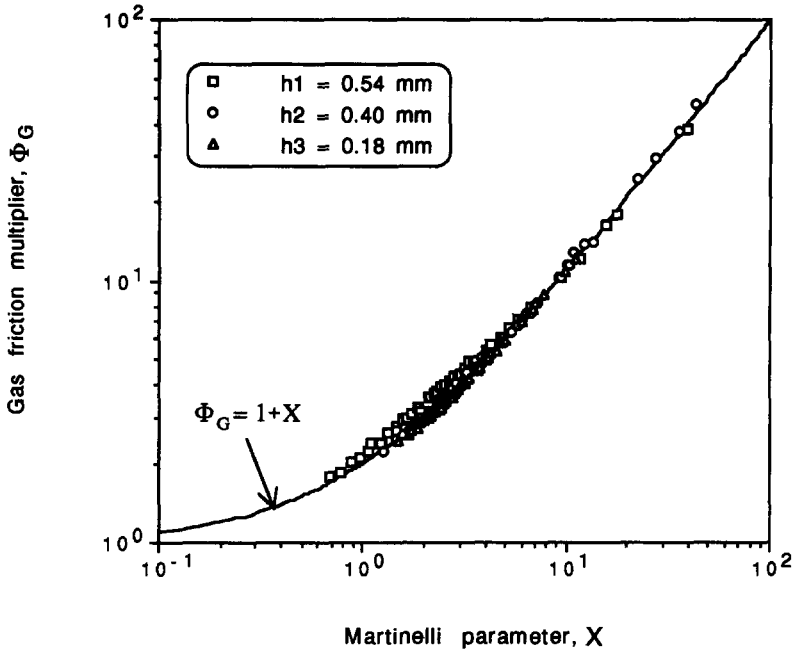

Figure 10. Gas friction multiplier vs Martinelli parameter (clay fracture).

Thus, from [14], [17] and [20], we deduce:

$$\frac{dP}{dx} = -\frac{12\mu_L V_L}{h^2\left(\frac{X}{1+X}\right)^2} \quad [21]$$

By comparing [12] and [21], the expression for the liquid volume fraction can be derived:

$$S_L = \left(\frac{X}{1+X}\right)^2 \quad [22]$$

A plot of the measured liquid volume fraction S_L versus the Martinelli parameter X is shown in figure 9. The curve of [22] is also plotted in figure 9. Values of the liquid volume fraction given by [22] are slightly higher than experimental values. This discrepancy is due to the fact that at the beginning of each experiment, the fracture was saturated with water. Therefore, capillary tubes for injection of gas-phase were partly occupied by water. When air injection started, water collected in the decanter came from both fracture and capillary tubes. The liquid volume in the decanter was then overestimated. As a result, the liquid volume fraction in the fracture was underestimated.

The plot of figure 10 displays Φ_G versus X for data obtained with the clay channel. This plot shows that the data follow the same equation [19] as for the glass channel. As the liquid volume fraction was not measured for the clay channel, we suppose that it is given by [22].

CHARACTERIZATION OF FLOW REGIMES

The establishment of previous relationships was based on the laminar flow hypothesis of each phase. In this section, we propose to verify the validity of this hypothesis.

By considering the two phases flowing in the fracture as a single-phase, we defined the mixture friction factor by:

$$\lambda_m = \frac{4h(-dP/dx)}{\rho_m V_m^2} \quad [23]$$

and the mixture Reynolds number by:

$$\mathrm{Re}_m = \frac{2h\rho_m V_m}{\mu_m} \quad [24]$$

where ρ_m is the mean density of the mixture:

$$\rho_m = S_L\rho_L + S_G\rho_G \quad [25]$$

V_m is the superficial velocity of the mixture:

$$V_m = V_L + V_g \quad [26]$$

and μ_m the dynamic viscosity of the mixture.

The above equations are similar to those defined for the homogeneous flow model. However, for our experimental data, the velocities for both phases are not equal.

Using [23]–[26], taking [12] into account and assuming that for a laminar flow regime the relationship between λ_m and Re_m is given by:

$$\lambda_m = \frac{96}{\mathrm{Re}_m} \quad [27]$$

we deduce the expression of the dynamic viscosity of the mixture:

$$\mu_m = \mu_L \frac{Q_L}{S_L(Q_L + Q_G)} \quad [28]$$

This expression of the dynamic viscosity of the mixture is unusual in the literature. However, taking [22] into account, [28] becomes:

$$\mu_m = \beta\mu_L + (1-\beta)\mu_G + 2\sqrt{\beta(1-\beta)\mu_L\mu_G} \quad [29]$$

where $\beta = Q_L/(Q_L + Q_G)$ is the homogeneous liquid volume fraction ($\beta \neq S_L$). It is interesting to compare the relationship [29] to the relationship proposed by Dukler *et al.* (1964) for two-phase flow in a pipe:

$$\mu_m = \beta\mu_L + (1-\beta)\mu_G \quad [30]$$

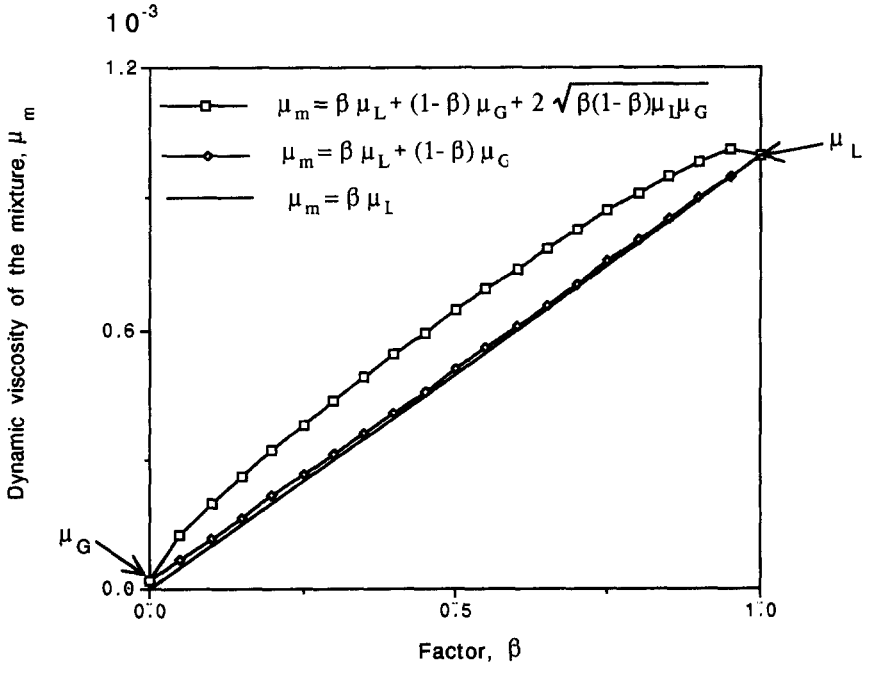

Figure 11. Dynamic viscosity of the mixture versus factor $\beta = Q_L/(Q_L + Q_G)$.

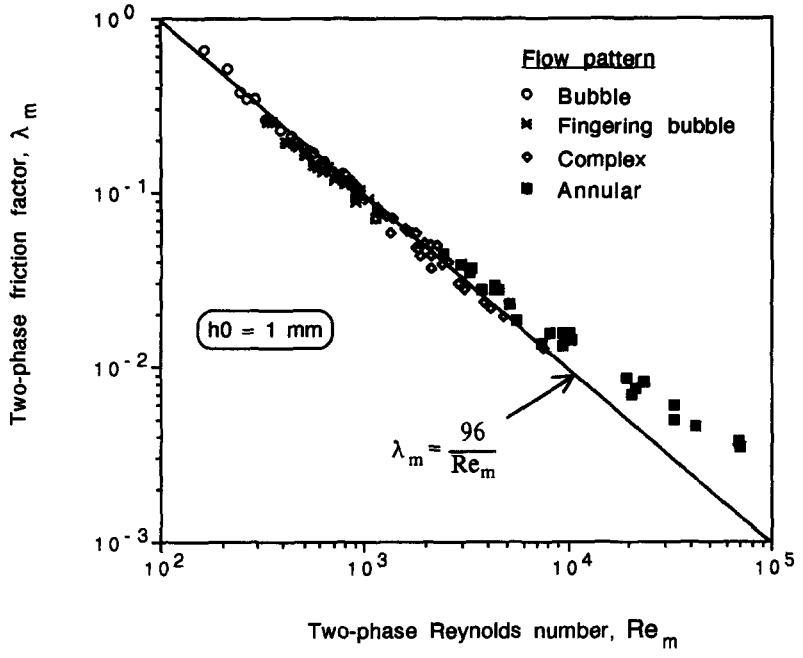

Figure 12. Two-phase friction factor (glass channel).

Curves of [29] and [30] are presented in figure 11. Because the dynamic viscosity of the gas is negligible in comparison with the dynamic viscosity of the liquid, [30] becomes:

$$\mu_m = \beta\mu_L \qquad [31]$$

In consequence of the square term [29] shows that $\forall\, \beta \in]0, 1[, \mu_m > \beta\mu_L$.

For data obtained with a glass channel, the plot of λ_m versus Re_m is shown in figure 12. Values of λ_m and Re_m were calculated using [28]. The curve of [27] is also plotted in figure 12. For $Re_m \leqslant 4000$, good agreement is obtained between experimental data and [27]. For $Re_m > 4000$ corresponding

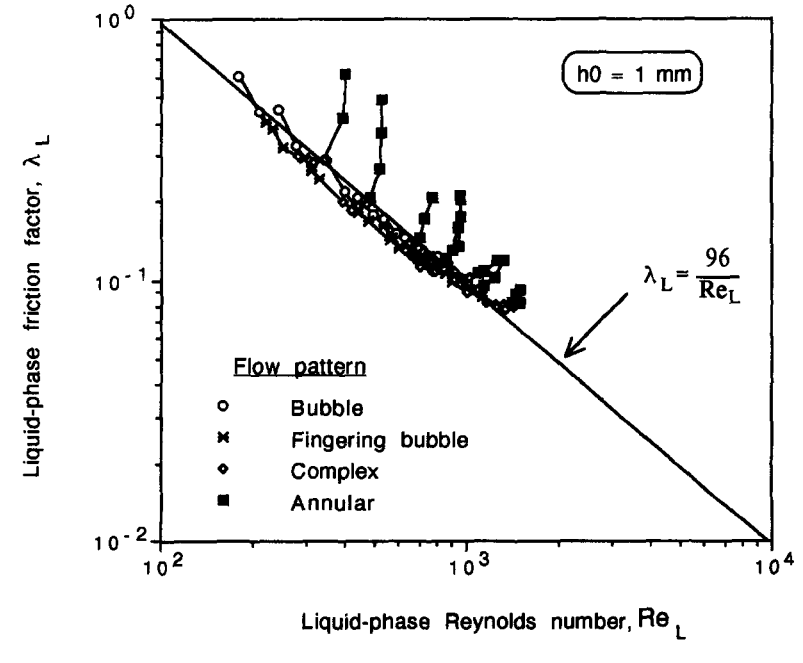

Figure 13. Liquid-phase friction factor (glass channel).

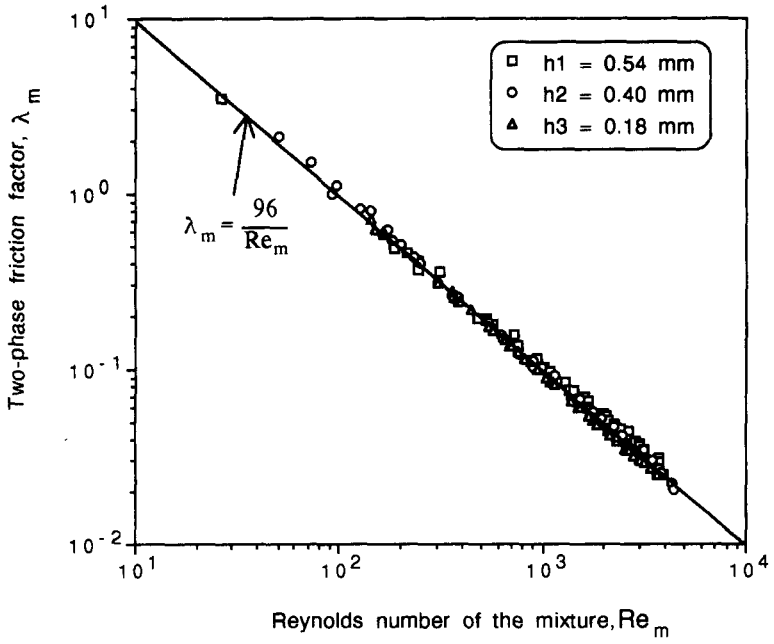

Figure 14. Two-phase friction factor (clay channel).

to annular flow, a deviation from [27] is observed. This deviation shows that for annular flow, the laminar hypotheses is not verified. This was confirmed by the analysis of the evolution of the liquid-phase friction factor:

$$\lambda_L = \frac{4h(-dP/dx)}{\rho_L U_L^2} \quad [32]$$

against the liquid-phase Reynolds number:

$$Re_L = \frac{2h\rho_L U_L}{\mu_L} \quad [33]$$

where U_L is the interstitial velocity defined by [9].

For laminar single-phase flow:

$$\lambda_L = \frac{96}{Re_L} \quad [34]$$

The plot of λ_L versus Re_L is shown in figure 13. Different curves were obtained. Each curve represents an individual experiment in which the liquid flow rate was held constant and the gas flow rate was increased. For a given liquid flow rate, at gas flow rates corresponding to bubbles, fingering bubbles and complex flow, the data follow the curve of [34]. At higher gas flow rates (annular flow), deviation from [34] is observed. As for single-phase flows, this deviation is caused by inertial forces.

For data obtained with the clay channel, the plot of λ_m versus Re_m is shown in figure 14. In this case, λ_m and Re_m were calculated by using [29]. The curve of the relationship [27] is also plotted in figure 14. Good agreement is obtained with experimental data and with the relationship [27].

THE GENERALIZED DARCY MODEL

If we consider that the capillary pressure is negligible in our experiments, the pressure gradient in each phase is then equal to the observed pressure gradient under two-phase conditions:

$$\frac{dP_L}{dx} = \frac{dP_G}{dx} = \frac{dP}{dx} \quad [35]$$

Relative permeabilities are then expressed from [1] and [2] for horizontal flow (no gravity):

$$Kr_L = -\frac{12\mu_L V_L}{h^2 \frac{dP}{dx}} \quad [36]$$

$$Kr_G = -\frac{12\mu_G V_G}{h^2 \frac{dP}{dx}} \quad [37]$$

By comparing [36] to [12] we deduce that the liquid-phase relative permeability is equal to the liquid volume fraction:

$$Kr_L = S_L \quad [38]$$

From the correlation between the gas and the liquid relative permeabilities:

$$\frac{Kr_L}{Kr_G} = \frac{\mu_L V_L}{\mu_G V_G} = X^2 \quad [39]$$

and taking [22] into account, the gas relative permeability can be derived:

$$Kr_G = (1 - \sqrt{S_L})^2 \quad [40]$$

For data obtained with the glass channel, the calculated Kr_L and Kr_G from [36] and [37] are plotted as functions of the measured liquid volume fraction in figure 15. Because the regime of annular flow experiments is not laminar, the corresponding data cannot be interpreted by using the generalized Darcy model. Therefore, these data are not plotted in figure 15. A good agreement is obtained between [38] and [40] and the data for laminar flow. These results are confirmed in figure 16 for the clay channel experiments. In this case, the liquid volume fraction was calculated by using [22].

Note that the sum of relative permeabilities is much less than 1 at intermediate liquid volume fraction, and not equal to 1 as it is commonly assumed. This implies that strong interference between phases occurs in the fracture.

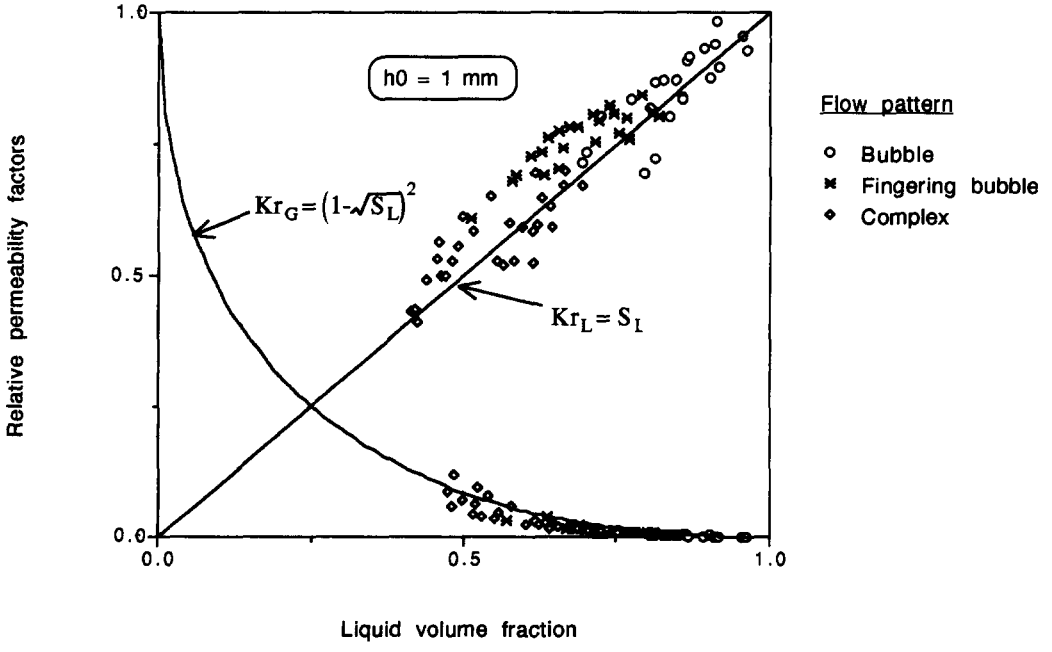

Figure 15. Relative permeabilities versus the liquid volume fraction (glass channel).

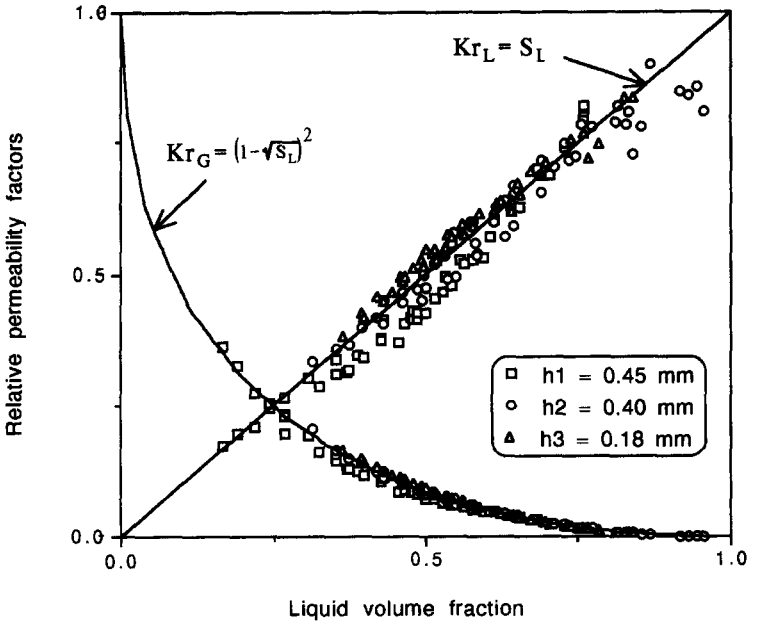

Figure 16. Relative permeabilities versus the liquid volume fraction (clay channel).

On the other hand, the parameter X in [39] is the same as the Martinelli parameter defined by [18]. In fact, comparison between [13], [14], [36] and [37], and taking [16] and [17] into account leads to the following relationships:

$$\Phi_L^2 = \frac{1}{Kr_L} \quad [41]$$

$$\Phi_G^2 = \frac{1}{Kr_G} \quad [42]$$

So in the case where the capillary pressure is negligible, the generalized Darcy model is analogous to the Lockhart & Martinelli model.

CONCLUSIONS

Two-phase (air–water) flow experiments were conducted in artificial horizontal fractures (narrow channels). Two experimental set-ups were utilized. One set of experiments was performed by using two glass plates. The second set of experiments was performed by using two bricks made of baked clay. The results of the experiments support the following conclusions:

(1) By varying the flow rates of each fluid phase, different flow structures were observed for the fracture made of glass (bubbles, fingering bubbles, complex, annular and droplet flow). These flow structures show more similarity to those observed in pipes than to those expected for porous media.
(2) Using the formalism developed for two-phase flow in pipes, and by taking experimental observations into account, a theoretical relationship for the two-phase pressure gradient was proposed. Good agreement was obtained between this relationship and experimental data for laminar flow regime.
(3) The Lockhart & Martinelli model gives a good fit for both pressure drop and liquid volume fraction against the Martinelli parameter at least for laminar flow regime.
(4) Considering the two phases flowing in the fracture as a single phase with averaged properties, the appropriate friction factor and Reynolds number of the mixture were defined. This model, which is similar to the homogeneous model, permits to select the experimental data corresponding to laminar flow regime.

(5) Using the generalized Darcy model, it was found that for a laminar flow regime, the liquid-phase relative permeability is equal to the liquid volume fraction; while the gas-phase relative permeability is not a linear function of the liquid volume fraction.

The experimental results were obtained with two kinds of fractures. However, only one combination of fluids was studied: air and water. The results must be expanded and generalized to other pairs of fluids.

Acknowledgements—This work was supported by the "Association de Recherche sur les Techniques d'Exploitation du Pétrole" (ARTEP) and the "Centre National de la Recherche Scientifique" (CNRS).

REFERENCES

Ali, M. I., Sadatomi, M., Charles, M. E. & Kawaji, M. 1991 Effects of gap width and orientation on two-phase flow in a narrow passage between two flat plates. In *Proceedings of the Int. Conference on Multiphase Flows*, Tsukuba, 24–27 September.

Coutris, N., Delhaye, J. M. & Nakach, R. 1989 Two-phase flow modelling: the closure issue for a two-layer flow. *Int. J. Multiphase Flow* **15,** 977–983.

Delhaye, J. M., Giot, M. & Riethmuller, M. L. 1981 *Thermohydraulics of Two-phase Systems for Industrial Design and Nuclear Engineering*, A von Karman Institute Book, pp. 206–207. McGraw–Hill, New York.

Dukler, A. E., Wicks, M. & Cleveland, R. G. 1964 Frictional pressure drop in two-phase flow: comparison of existing correlation or pressure loss and hold-up. *AIChE Jl* **10,** 38–43.

Fourar, M., Bories, S., Lenormand, R. & Persoff, P. 1993 Two-phase flow in smooth and rough fracture: measurement and correlation by porous-media and pipe-flow models. *Wat. Resour. Res.* **29,** 3699–3708.

Fourar, M., Piquemal, J. & Bories, S. 1991 Ecoulement diphasique bidimensionel plan liquide– gaz. II: gradients de pression et fractions volumiques des phases d'un écoulement horizontal. *C.R. Acad. Sci. Paris* **313,** 477–480.

Lockhart, R. W. & Martinelli, R. C. 1949 Proposed correlation of data for isothermal two-phase, two-component flow in pipes. *Chem. Engng Prog.* **45,** 39.

Persoff, P., Pruess, K. & Myer, L. 1991 Two-phase flow visualization and relative permeability measurement in transparent replicas of rough-walled rock fractures. Presented at the *Sixteenth Stanford Geothermal Workshop*, Stanford University, 25–27 January.

Persoff, P., Pruess, K. & Myer, L. 1994 Method apparatus for determining two-phase flow in rock fracture. U.S. Patent 5,311,766, 17 May.

Pruess, K. & Tsang, Y. V. 1990 On two-phase relative permeability and capillary in rough-walled rock fractures. *Wat. Resour. Res.* **26,** 1915–1926.

Pyrak-Nolte, L. J., Helgeson, D., Haley, G. M. & Morris, J. W. 1992 Immiscible fluid flow in a fracture. In *33rd Rock Mechanics Symposium*, pp. 571–578.

Romm, E. S. 1966 Fluid flow in fractured rocks. Nedra, Moscow (in Russian; English translation, W. R. Blake, Bartlesville, OK, 1972).